

Investigation of the Protective Effect of Extracellular Vesicle miR-124 on Retinal Ganglion Cells Using a Photolabile Paper-Based Chip

Yi-Hsun Chen,^{1,2} Yu Chuan Huang,^{3,4} Chih-Hung Chen,² Yao-Tseng Wen,⁵ Rong-Kung Tsai,^{5,6} and Chihchen Chen¹

¹Institution of NanoEngineering and MicroSystems, Department of Power Mechanical Engineering, National Tsing Hua University, Hsinchu, Taiwan

²Biomedical Technology and Device Research Laboratories (BDL), Industrial Technology Research Institute (ITRI), Hsinchu, Taiwan

³School of Pharmacy & Institute Pharmacy, National Defense Medical Center, Taipei, Republic of China

⁴Department of Research and Development, National Defense Medical Center, Taipei, Republic of China

⁵Institute of Eye Research, Buddhist Tzu Chi General Hospital, Hualien, Taiwan

⁶Institute of Medical Sciences, Tzu Chi University, Hualien, Taiwan

Correspondence: Chihchen Chen, Institution of NanoEngineering and MicroSystems, Department of Power Mechanical Engineering, National Tsing Hua University, No. 101, Section 2, Kuang-Fu Road, Hsinchu 300044, Taiwan R.O.C., Taiwan; chihchen@mx.nthu.edu.tw.

YHC and YCH contributed equally to this study.

Received: July 6, 2022

Accepted: December 18, 2022

Published: January 23, 2023

Citation: Chen YH, Huang YC, Chen CH, Wen YT, Tsai RK, Chen C. Investigation of the protective effect of extracellular vesicle miR-124 on retinal ganglion cells using a photolabile paper-based chip. *Invest Ophthalmol Vis Sci.* 2023;64(1):17. <https://doi.org/10.1167/iovs.64.1.17>

PURPOSE. Photolabile paper-based chips were developed to isolate extracellular vesicles (EVs) from small-volume samples (less than 30 μ L), such as vitreous humor. Putative neuroprotective effects of EVs' microRNAs were investigated by using the paper chip and a rodent model with nonarteritic anterior ischemic optic neuropathy (rNAION).

METHODS. rNAION was established using laser-induced photoactivation of rose bengal administered intravenously. On days 0, 0.25, 1, 3, and 7 after rNAION induction, CD63-positive EV microRNAs (CD63⁺-EV miRNAs) in vitreous humor samples were enriched using the paper chip and assessed using microarray and quantitative RT-PCR analyses. The viability and visual function of retinal ganglion cells (RGCs) were further assessed by measuring photopic flash visual evoked potentials (FVEPs).

RESULTS. We identified 38 different variations of CD63⁺-EV miRNAs with more than twofold altered expressions. Among them, M1-related miRNA, miR-31a-5p, and M2-related miRNA, miR-125a-5p, miR-182, miR-181a-5p, and miR-124-3, were capable of coordinating anti-inflammatory reactions during rNAION because of their capacity to activate macrophages. In particular, miR-124, having the most dramatic alteration of gene expression, was synthesized and injected intravitreally. Compared to controls, rats that received miR-124 had shown increased RGC survivability and improved visual function.

CONCLUSIONS. Our research team has developed a paper-based chip capable of capturing EVs that can be released after UV exposure. The quantity and quality of EV-miRNAs extracted are adequate for microarray and quantitative RT-PCR analyses. Animal studies suggest that miR-124 may play a neuroprotective role in the natural recovery of rNAION and holds the potential to be a novel treatment option.

Keywords: photolabile paper-based chip, CD63-positive extracellular vesicles (CD63⁺-EVs), nonarteritic anterior ischemic optic neuropathy (NAION), miR-124, flash visual evoked potential (FVEP)

Nonarteritic anterior ischemic optic neuropathy (NAION) is the most common cause of optic neuropathy in patients over 50 years of age with an incidence of 2.3 to 10.2 cases per 100,000 persons every year in the United States.^{1,2} NAION typically presents as acute and painless monocular vision loss. Although the exact mechanism is unclear, NAION results in optic nerve edema, selective loss of the retinal ganglion cell neurons (RGCs) from acute ischemia, and atrophy of the optic nerve head.^{3,4} There is currently no known effective treatment to reduce the degree of visual impairment in acute NAION. Rodent models of NAION (rNAION) can be induced noninvasively by using laser exposure to generate superoxide radicals that result in damaged capil-

lary endothelium and ischemia to the optic nerve head. The rNAION model features an early optic nerve injury, inflammation, and RGC loss, which closely resembles the presentation and physiologic responses of human NAION.^{5,6}

We and others have found that introducing the granulocyte-colony stimulating factor (G-CSF) into vitreous humor could significantly protect microglia and vision by reducing M1-phase macrophage infiltration after rNAION.^{2,3} The protection effect of G-CSF on the optic nerves was thought to be associated with increased mRNA levels of M2-macrophage markers (e.g., Arg1, CD206, and Fizz1) and decreased M1 mRNA markers (e.g., CD32 and CD86).^{2,7} To further elucidate the role of G-CSF, we set out to investigate

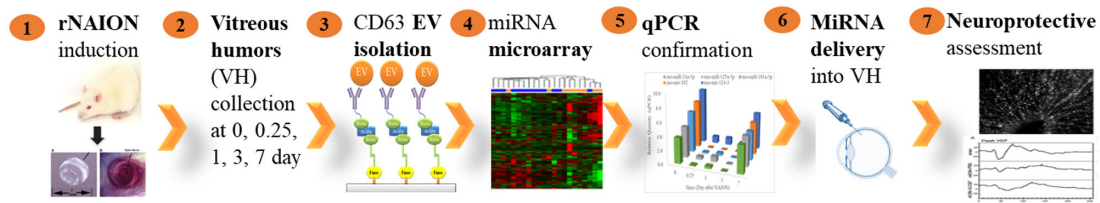


FIGURE 1. Flowchart of the miR-124 discovery process. CD63⁺-EV extraction from the VH of rNAION animals at days 0, 0.25, 1, 3, and 7 by photolabile chips and then released from the chip by UV light. Total RNA was extracted from isolated EVs for miRNA microarray analysis. Some significantly altered miRNAs were confirmed by qPCR. miR-124 was synthesized and injected into rNAION animals. Finally, miR-124 was found to have the potential to promote neuroprotective effects by stabilizing FVEP functions and offering RGC protection.

microRNAs (miRNAs), especially those carried by extracellular vesicles (EVs) that may regulate downstream mRNAs in M1/M2 macrophages during natural recovery from rNAION. The quick onset of inflammatory M1 macrophages followed by the infiltration of anti-inflammatory M2 macrophages after rNAION may be modulated by different groups of miRNAs.

Extracellular vesicles carry diverse cargo, including proteins, lipids, and genetic materials that are associated with their parental cells. It is becoming increasingly clear that EVs play a unique and critical role in cell-to-cell signaling through the delivery of their cargo to target cells.^{8,9} EVs are lipid-binding vesicles secreted by cells into the extracellular space and are differentiated according to their biogenesis, release pathways, size, content, and function. The three main subtypes of EVs are exosomes (50–200 nm), microvesicles (200–1000 nm), and apoptotic bodies (800–5000 nm). Not surprisingly, EVs also have a wide range of biological functions in eye diseases, including diabetic retinopathy, age-related macular degeneration, autoimmune uveitis, glaucoma, traumatic optic neuropathies, corneal diseases, retinopathy of prematurity, and uveal melanoma.^{10–13} Mesenchymal stem cell-derived exosome is a neuroprotective factor capable of significantly attenuating neuronal damage after ischemia.¹⁴ In this study, we aim to explore the potential roles of EV miRNAs in NAION. EVs can be characterized by their density, lipid composition, and distinctive surface molecules such as tetraspanins.¹⁵ CD9, CD63, and CD81 are major tetraspanin proteins found on EVs, with CD63 being one of the most abundant and well-known biomarkers on EV membranes.^{16–18} In our previous research, CD63-positive EVs (CD63⁺-EVs) were found in aqueous humor samples.¹⁹

However, current EV isolation methods typically require sample volumes of 100 μ L or larger, including ultracentrifugation, size exclusion chromatography, ultrafiltration, and sedimentation.^{20–22} To isolate EVs from biological samples as small as 30 μ L, such as biopsy from aqueous humor and vitreous humor, we developed a novel method using the chemically modified cellulose paper-based chips. Capture molecules, such as anti-CD63 antibodies, can be immobilized at a high density owing to the large surface-to-volume ratio, thereby increasing capture capacity and efficiency. A UV-sensitive linker was employed, allowing to release captured EVs easily after a brief UV exposure.

In recent years, circulating miRNAs have emerged as promising diagnostic and prognostic biomarkers for the detection of diseases, because of their high specificity and sensitivity. More important, specific miRNA expression profiles reflect not only the existence of early-stage diseases but also the dynamic development of advanced-

stage diseases.²³ EV miRNAs have been shown to regulate overactive immune responses and RGC cell apoptosis, which may be especially important in the occurrence and development of neurologic diseases.^{24,25} It is possible to use miRNAs as biomarkers and in the development of novel treatments. Endogenous miRNAs are already widely used as biomarkers in specific in vivo animal models of neurodegenerative diseases.^{26–29} Further understanding of the interplay between miRNA profiles and the recovery period in rNAION may lead to the discovery of novel therapeutic approaches. A flowchart of our miRNA discovery process is shown as Figure 1. We hypothesize that EV miRNA patterns may be altered in rNAION and aim to discover their potential roles in the RGC survival and recovery of visual function.^{30,31}

EXPERIMENTAL

Animal and Study Design

We first used New Zealand White (NZW) rabbits for assessing the performance of paper chips, as ca. 200 μ L aqueous humor sample per eye could be obtained from rabbits compared to only 10 μ L from rats. Afterward, vitreous humor samples from NAION-induced adult male Wistar rats (rNAION) were used. Rats weighed 150 to 180 g, were 7 to 8 weeks old, and originated from the breeding colony of BioLASCO Co. (Taipei, Taiwan). Animal care and experimental procedures were performed in compliance with the ARVO Statement for the Use of Animals in Ophthalmic and Vision Research with IACUC approval no. 109-25. All procedures were performed on animals under anesthesia achieved by intramuscular administration of ketamine and xylazine (80 mg/4 mg/kg body weight; Sigma, St. Louis, MO, USA). We chose to study vitreous humor, mainly because of their close proximity with RGCs; hence, EVs inside may reflect the status of RGCs more closely than those in aqueous humor.

Induction of Nonarteritic Anterior Ischemic Optic Neuropathy in Rodents

To identify miRNA profiles during the natural recovery period, rats were induced with NAION and their vitreous humor samples were collected on days 0, 0.25, 1, 3, and 7 after induction. rNAION was established based on previously used methods.^{32–34} Briefly, anesthesia was established using ketamine–xylazine 80 mg/4 mg/kg intramuscularly. Pupils were dilated with cyclopentolate–phenylephrine 1% to 2.5% topically. Then, 1 mL/kg of 2.5 mM rose bengal (Sigma-Aldrich) in Dulbecco's phosphate-buffered saline (D-PBS; pH 7.4) was administered intravenously through the tail vein. Thirty seconds postinjection of rose bengal,

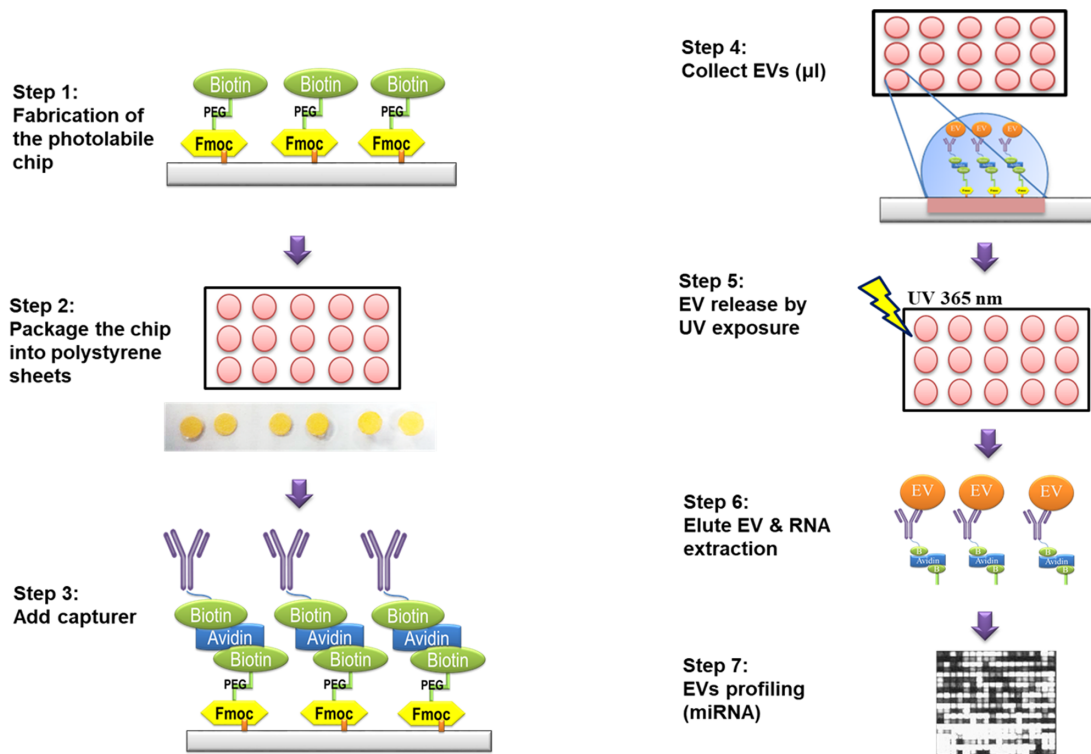


FIGURE 2. Steps to prepare photolabile chips and obtain CD63⁺-EVs.

a photosensitizing agent, the capillaries of the optic nerve head eye were illuminated by a 532-nm argon laser (NIDEK MC-500 Vixi; Nidek Co., Ltd. Gamagori, Japan). The illumination was 500 μm in size, 80 mW in power, and 1 second in duration for 12 pulses. This produces free radicals in the optic nerve head, creating an oxidative stress environment followed by ischemic optic neuropathy and RGC death.^{1-4,32-34} Subsequent bright golden color of capillaries demonstrated successful activation of rose bengal and resultant ischemia to the optic nerve head in the rNAION group ($n = 15$). In the sham group ($n = 15$), rats were exposed to the same laser without administration of rose bengal.

Preparation of the Photolabile Chip for Collecting CD63⁺-EVs

The preparation and operation of the photolabile chip are shown schematically in Figure 2.³⁵⁻³⁷ First, 5-mm-diameter holes were made on polystyrene sheets and 5.2-mm-diameter paper chips were chemically modified. The detailed preparation method is described in Supplementary Figure S1. Then, the chips were placed between two polystyrene sheets, centered over the holes, and heat laminated. This is analogous to assembling the same layout as a 96-well microtiter plate. Each chip was blocked with 10 μL 1% (w/v) bovine serum albumin (BSA) (Aldrich Chemical Co., Milwaukee, WI, USA) in phosphate-buffered saline (PBS) for 3 minutes. BSA was then replaced with 10 μL of 20 $\mu\text{g}/\text{mL}$ biotinylated anti-CD63 antibody (containing 1% (w/v) BSA and 0.09% (w/v) sodium azide solution) and reacted for 5 minutes. Each chip was washed three times with PBS (Aldrich Chemical Co.) and ready to perform CD63⁺-EV extraction (Fig. 2, steps 1–3). We had to ensure that BSA and PBS did not produce a large background by filtering

0.02 μm ; the signal is the same as EVs treated with 0.5% nonionic detergent Nonidet P-40 for 30 minutes at room temperature using NTA (NS 300; Malvern, Worcestershire, UK) and the MKII imaging flow cytometer (Amnis MKII; Luminex, Austin, Texas, USA) (data not shown). The samples of vitreous humor were spotted on the photolabile chip at a rate of 10 μL per 20 seconds or three times per minute. Then, the chip was washed with 20 μL PBS six times. PBS was placed on the top surface of the chip, allowing the substance to pass through the chip by gravity, and collected at the bottom. The chip was then exposed to 365 nm UV light for 5 minutes in B2 BioSafety Cabinets (Thermo Fisher Scientific, Inc., Waltham, Massachusetts, USA) to break the photolabile links. CD63⁺-EVs were collected by washing the chip with 20 μL PBS six times (Fig. 2, steps 4–7). An imaging flow cytometer and paper-based ELISA were used to validate CD63⁺-EVs from the chip (data not shown). All samples were stored at -80°C until use.

Extraction of Total RNA From CD63⁺-EVs

Total RNA, including small RNAs, was isolated from CD63⁺-EVs using modified Qiagen's miRNeasy kit (Venlo, Netherlands) (miRNeasy Serum/Plasma Kit, cat. 217184). Briefly, 80 μL PBS and 1 mL Qiazol solution were added to 120 μL of the extracted EV sample. Samples were shaken and allowed to react at room temperature for 5 minutes, which separated proteins from nucleic acid molecules. Then, 200 μL chloroform was added to the samples and shaken vigorously for 15 seconds to isolate RNA from other nucleic acids. All samples were centrifuged at $13,000 \times g$ for 15 minutes at 4°C to partition purified RNAs to the upper layer. Purified RNA was isolated and air-dried. Finally, total RNA was dissolved in a preservation solution, and its

concentration and purity were analyzed with OD 260/280. Quantification and quality check of isolated miRNA was performed on 2100 BioAnalyzer (Agilent, Santa Clara, California, USA) using small RNA microfluidics chips. The extracted total RNA solutions were stored at -20°C until use.

miRNA Array Probe Labeling and Analysis

Labeled probes were hybridized to Thermo Fisher miRNA Array 4.0 using the standard procedure. The total data set included 1218 miRNAs (rat only), and the sample input required 130 ng total RNA. Upon scanning the hybridized and washed chips, data were obtained in a set of data files (.cel, .arr, .jpg). The signals detected by the probes were stored as CEL files and were analyzed with the Expression Console and Transcriptome Analysis Console software. After importing CEL files, the RMA-DABG summarization algorithm was applied using the Expression Console with “only *Rattus norvegicus*” applied. The related quantity (RQ) of miRNA expression was normalized using the robust multi-array average (RMA) method.³⁸ The RMA algorithm fits a robust linear model at the probe level to minimize the effect of probe-specific affinity differences. Expressions of genes for each group (on days 0, 0.25, 1, 3, and 7 after induction) were evaluated and presented in \log_2 fold changes over the baseline (on day 0, before rNAION induction).

miRNA Analysis Validated by Semiquantitative RT-PCR

Five miRNAs related to M1 and M2 macrophage inflammatory modulation were selected to be further quantified: miR-125a-5p, miR-31a-5p, miR-182, miR-124-3, and miR-181a-5p.^{31,39,40} Primers were synthesized and miRNA expressions were quantified using TaqMan PCR kits from Thermo Fisher Scientific. Quantitative RT-PCR (RT-qPCR) was executed on an Applied Biosystems 7900HT Sequence Detection System (P/N: 4329002; Applied Biosystems, Waltham, Massachusetts, USA). Stem-loop primer sequences used in RT-qPCR experiments are listed in Table 1. The 10- μL PCR reaction mixture includes 0.67 μL RT product, 1 \times TaqMan Universal PCR Master Mix (P/N: 4324018; Applied Biosystems), 0.2 μM TaqMan probe, 1.5 μM forward primer, and 0.7 μM reverse primer. The reaction was performed in a 384-well plate at 95°C for 10 minutes, followed by 40 cycles at 95°C for 15 seconds and 60°C for 1 minute. GAPDH was used as a cell-free internal control and U6snRNA as an inter-

nal standard to determine relevant quantities. All reactions were processed in triplicate.

Treatment With Synthesized miR-124 in rNAION

After identifying miR-124 as a possible treatment, NAION was induced in the same manner in another group of rats (as shown in “Induction of Nonarteritic Anterior Ischemic Optic Neuropathy in Rodents”). After the general anesthesia, eyes were applied with Alcaine, Mydrin-P, and 5% povidone-iodine. Intravitreal injections were performed under sterile conditions, using a dissecting microscope to avoid damage to the lens and retina. The rats in the synthetic miR-124-treated group (5 μL , 10 μM , $n = 6$) or in the control PBS-treated group (5 μL PBS, $n = 6$) were administered intravitreally by using a 33-gauge needle attached to a 10- μL Hamilton Gastight syringe (Hamilton 1701RN SYR; Hamilton Co., Hamilton, KS, USA).

Measurement of the Viability of RGCs by Retrograde Labeling With Fluoro-Gold

Four weeks after administration, half of the rats ($n = 3$) from each group had their experimental eyeball ($n = 3$) harvested to measure RGC density, and the other half ($n = 3$) had their visual function assessed by photopic flash visual evoked potentials (FVEPs) (see “FVEPs”).^{2,4,33,34,41} Three rats were selected from each group by stratified random sampling. To avoid overcounting RGCs by mixing labeled RGCs with dye engulfing macrophages and microglia, retrograde labeling was performed 1 week prior to assessment. Briefly, the skin covering the skull of the rats was opened and 1.5 μL 5% Fluoro-Gold was injected into each side of the superior colliculus with a Hamilton syringe. The eyeballs were harvested and the rats were euthanized after 1 week. RGC densities were studied on retinal flat-mounts of the central retina at a distance between 1 and 3 mm from the optic nerve head.

FVEPs

Four weeks after rAION induction ($n = 3$), the rat skin over the skull was opened to expose the sagittal coordinates for implanting two electrodes at the primary visual cortex region of both hemispheres (AP (anterior-posterior): -8 mm, ML (medial-lateral): -3.0 mm). Another electrode was set at the frontal cortex (AP: 3 mm). The electrode at the primary

TABLE 1. miRNA Primers of *Rattus Norvegicus* Used in TaqMan Quantitative PCR Experiments

Stem-Loop ID	Stem-Loop Sequence	miRBase ID	Mature miRNA Sequence
rno-mir-124-1	AGGCCUCUCUCUCCGUGUUCACAGCGGACCUUGAU UUAAAUGUCCAUAACAUAUAAAGGCACGCGGUGAAU GCCAAGAAUGGGGCGUG	rno-mir-124-3p	UAAGGCACGCGGUGAAUGCC
rno-mir-182	ACGCGGGUCUAGCUGCCGGAGGCCUCCACCGU UUUUGGCAAUGGUAGAACUCACACCGGUA	rno-mir-182	UUUGGCAAUGGUAGAACUCACACCG
rno-mir-125a	UGCCGGCCUCUGGGUCCUGAGACCCUUUAACC UGUGAGGACGUCCAGGGUCACAGGUGAGGUUCU GGGAGCCUGGCGCCUGGC	rno-mir-125a-5p	UCCUGAGACCCUUUAACCUGUGA
rno-mir-181a-1	AGGUUGCUUCAGUGAACAUUCAACGUGUCGGU GAGUUUGGAAUUAACAUAUAAAACCAUCGACCGUU GAUUGUACCCUAUAGCUAACCAUUAUCUACUCC	rno-mir-181a-5p	AACAUUCAACGUGUCGGUGAGU
rno-mir-31a	UGUCCUGAAACUUGGAACUGGAGAGGAGGCAA GAUGCUGGCAUAGCUGUUGAACUGAGAACCUGCUAU GCCAACAUUUGCCAUCUUCCUGUCUGACAGCAGCU	rno-mir-31a-5p	AGGCAAGAUGCUGGCAUAGCUG

visual cortex was the active (positive) electrode, the electrode at the frontal cortex was the reference (negative) electrode, and the ground electrode was connected to the rat tail. The FVEP was measured by using a visual electrodiagnostic system (Espion; Diagnosys LLC, Gaithersburg, MA, USA). The FVEPs were recorded under no background illumination, with a flash intensity of 30 cd·s/m² and a single flash with a flash rate of 1.02 Hz, respectively. We plotted the average of 64 sweeps on a graph. The amplitudes of the first positive peak (P1) and second negative peak (N2) of FVEP were recorded and analyzed. The wave height of P1–N2 was compared between groups to evaluate the visual function.^{2,4,33,34,41}

RESULTS

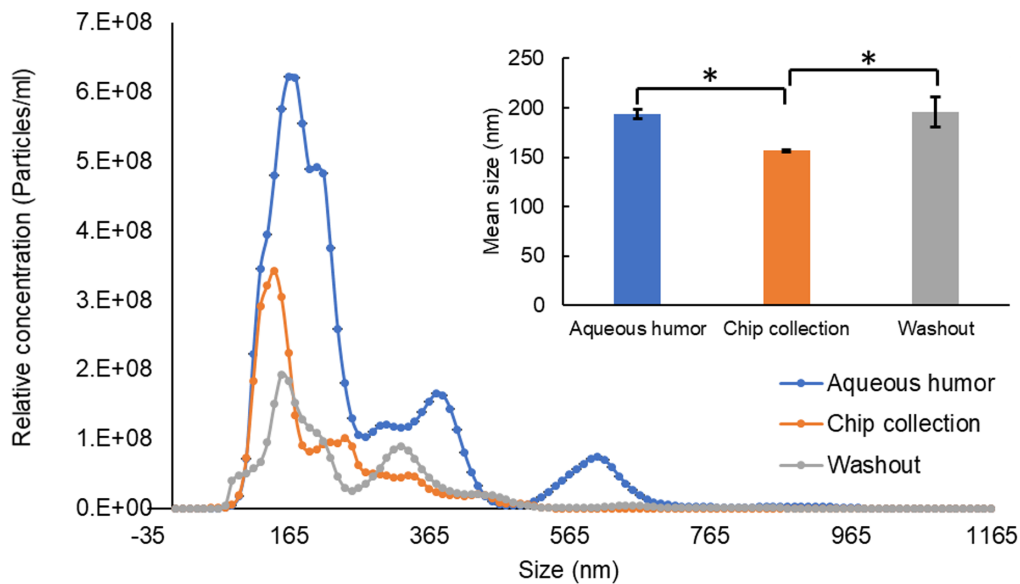
Photolabile Chips Used to Extract CD63⁺-EVs From NZW Rabbits' Aqueous Humor

We developed a low-volume EV extraction technique using photolabile paper conjugated with CD63 monoclonal antibodies to capture CD63⁺-EVs (as shown in Fig. 2). To validate the experimental procedure, 30 μ L of NZW rabbit aqueous humor samples was applied to the photolabile chip. The size distribution of CD63⁺-EVs collected and released from the chip was compared with that from the original sample and the washout uncaptured fluid. The size distribution and particle concentration were determined by using nanoparticle tracking analysis (NTA). Samples were vortexed

and diluted in particle-free PBS (0.02 μ m filtered) to be within a recommended concentration range (1~10 \times 10⁸ particles/mL). Samples were analyzed using NTA 3.1 Build 3.1.45 software (NS300; Malvern), with a camera level of 15 to 16 and a detection threshold of 5. The mean size of EVs in the original aqueous humor (254.8 \pm 13.0 nm) and washout (241.4 \pm 17.2 nm) was both larger than that of EVs collected by chip (202.1 \pm 0.3 nm), $P < 0.01$ (Fig. 3). In this study, a supernatant containing “buoyant” vesicles we directly gained following 30 minutes of centrifugation at 2000 \times g and 30 minutes at 12,000 \times g from vitreous humor (VH) of experimental rats only allowed us to take away cellular and vitreous debris. Our initial VH should have had all kinds of EVs (exosomes and microvesicles). The size was slightly larger. But with the passed paper-based CD63⁺-EV isolated chip, the size got smaller. We also found that the mean size of CD63⁺-EVs was approximately 100 nm by examining transmission electron microscopy (TEM) (HT7800; Hitachi, Chiyoda, Tokyo, Japan) (data not shown).

Total RNA Extracted From CD⁺63 EVs Collected by Chips in rNAION Rats

For the sham group ($n = 3$) and rNAION ($n = 3$), 10 μ L vitreous humor was collected from each study eye on days 0, 0.25, 1, 3, and 7 after rNAION induction. Vitreous humor from each group was pooled (30 μ L) at five intervals and applied to the paper chip ($n = 1$, five intervals) for the proof-of-principle data set by both groups.



Particle size (nm)	Aqueous humor (AH)	Photolabile chip	Washout samples
Statics	Mean \pm SD		
Mean	254.8 \pm 13	202.1 \pm 0.3	241.4 \pm 17.2
D10	131.6 \pm 10.5	112.8 \pm 4	123.3 \pm 6.4
D50	193.9\pm4.8	156.4\pm1	196.1\pm15.1
D90	438.6 \pm 51.8	320.8 \pm 11.3	376.2 \pm 24.6

FIGURE 3. The photolabile chips eluted EV-sized particles through a photocleavable linker. Aqueous humor: original particle size distribution of NZW rabbit aqueous humor. Chip collection: the chip collected particle size distribution of NZW rabbit aqueous humor. Washout samples: the washout fluid collected particle size distribution of NZW rabbit aqueous humor. * $P < 0.05$.

TABLE 2. Quantity and Quality of RNA From CD63⁺-EVs Captured by Photolabile Chips

Group	Concentration (ng/μL)	OD 260/280	Total Yield (ng)	Volume (μL)	Original Volume (μL)	Original Concentration (ng/μL)
D0	60.3	1.6	723.6	12	30	24.1
D0.25	16	1.54	192	12	30	6.4
D1	38.7	1.62	464.4	12	30	15.5
D3	33.5	1.56	402	12	30	13.4
D7	21.4	1.66	256.8	12	30	8.56

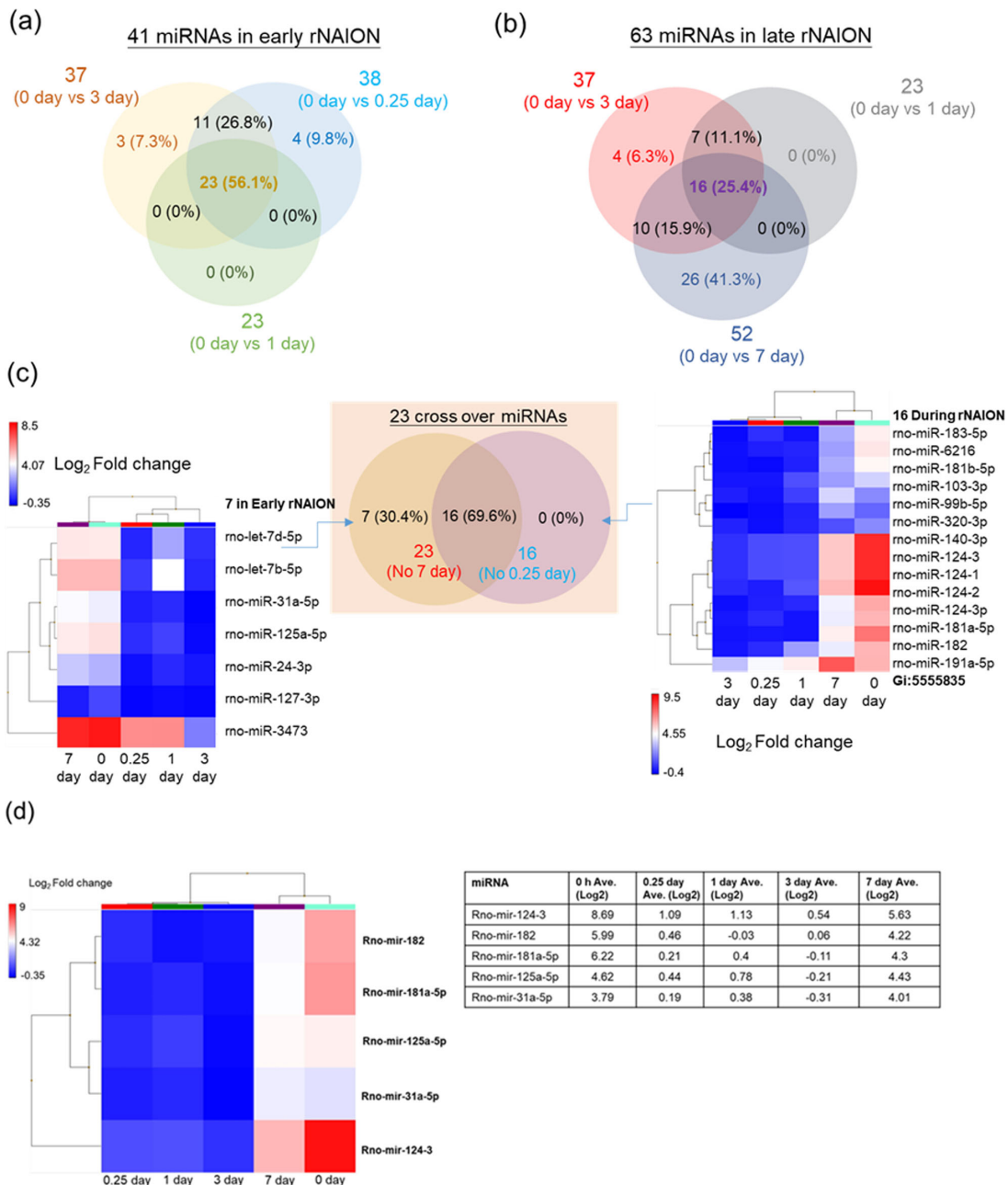


FIGURE 4. Heatmap and Venn diagram of selected miRNA expression profiles in different stages of rNAION in CD63⁺-EVs in vitreous humor. (A) Forty-one early-stage miRNAs. (B) Sixty-three late-stage miRNAs. (C) Twenty-three crossover miRNAs. (D) Heatmap of five selected M1- and M2-associated miRNA expression profiles in CD63⁺-EVs from rNAION vitreous humor at different natural recovery times. Red indicates high expression levels, and blue indicates low expression levels.

The total RNA from the isolated CD63⁺-EVs was reconstituted in PBS. The miRNA purity (ratio of OD 260/280) was between 1.54 and 1.66. The amount of miRNA was between

192 and 723.6 ng (Table 2). In total, 130 ng RNA (OD 260/280 ratio >1.5) was used for the microarray analysis (Thermo Fisher GeneChip miRNA 4.0).

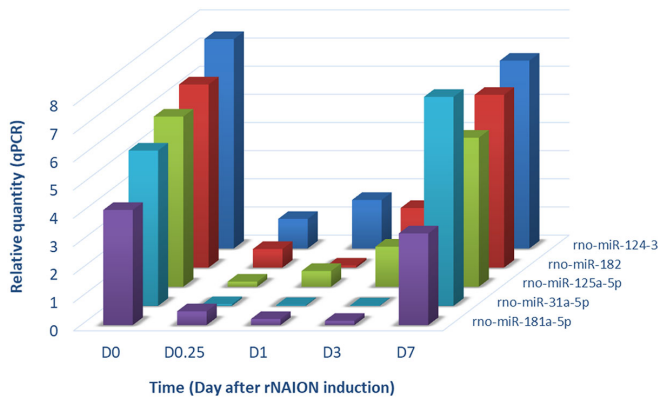


FIGURE 5. miRNA change determined by quantitative PCR in rNAION after natural recovery.

miRNA Profiles During Natural Recovery in rNAION

We analyzed miRNA expressions throughout the natural recovery period on days 0, 0.25, 1, 3, and 7 ($n = 1$ for each time interval). Principal component analysis showed that gene expression on day 7 was close to the baseline sample (day 0, no induction of rNAION) and 74.5% at principal component analysis 1 (Supplementary Fig. S2A). Compared to the baseline sample, 38 of the 1218 miRNAs probes of *Rattus norvegicus* analyzed showed a significant difference in expression levels (more than twofold; Supplementary Fig. S2B); their miRNA name (transcript ID) can be checked by their ID in Supplementary Table S1. The number of significantly altered miRNAs compared to day 0 was 28, 22, 27, and

41 on days 0.25, 1, 3, and 7, respectively (Supplementary Fig. S3A). Among them, 31 miRNAs were upregulated; however, 27 of these were expressed only on day 7. On days 0.25, 1, and 3, the number of significantly upregulated miRNAs was 2, 2, and 1, respectively (Supplementary Fig. S3B). Twenty-eight miRNAs were downregulated. On days 0.25, 1, 3, and 7, the number of significantly downregulated miRNAs was 26, 20, 27, and 12, respectively (Supplementary Fig. S3C).

Heatmap From Significantly Altered miRNAs in rNAION During the Natural Recovery Period

Our previous research showed that the immune response near the optic ganglia was due to M1-related monocyte activation in rNAION. During the natural recovery period of rNAION, both M1- and M2-related miRNAs were downregulated early and upregulated to baseline by day 7. In Figures 4A–C, 23 miRNAs are shown in early rNAION (excluded day 7), while 16 miRNA profiles are shown throughout the recovery period of rNAION. Interestingly, one M1-related miRNA (miR-31a-5p) and four M2-related miRNAs (miR-125a-5p, miR-124-3, miR-182, and miR-181a-5p) were significantly downregulated in early rNAION and then recovered to baseline at day 7 (Fig. 4D). The optic nerve damage caused by macrophage activating factors may be regulated by miRNAs. In this study, 38 miRNA expressions were significantly altered in CD63⁺-EVs of the vitreous humor. Among them, five were selected for further analysis for their potential involvement in M1 and M2 modulation.^{42,43} M1/M2 macrophage-related miRNAs (e.g., miR-125a-5p, miR-31a-5p, miR-124-3, miR-182, and miR-181a-5p) were downregulated in the first 3 days but returned to the baseline on day 7. Of these, miR-124-3 was significantly downregulated on day

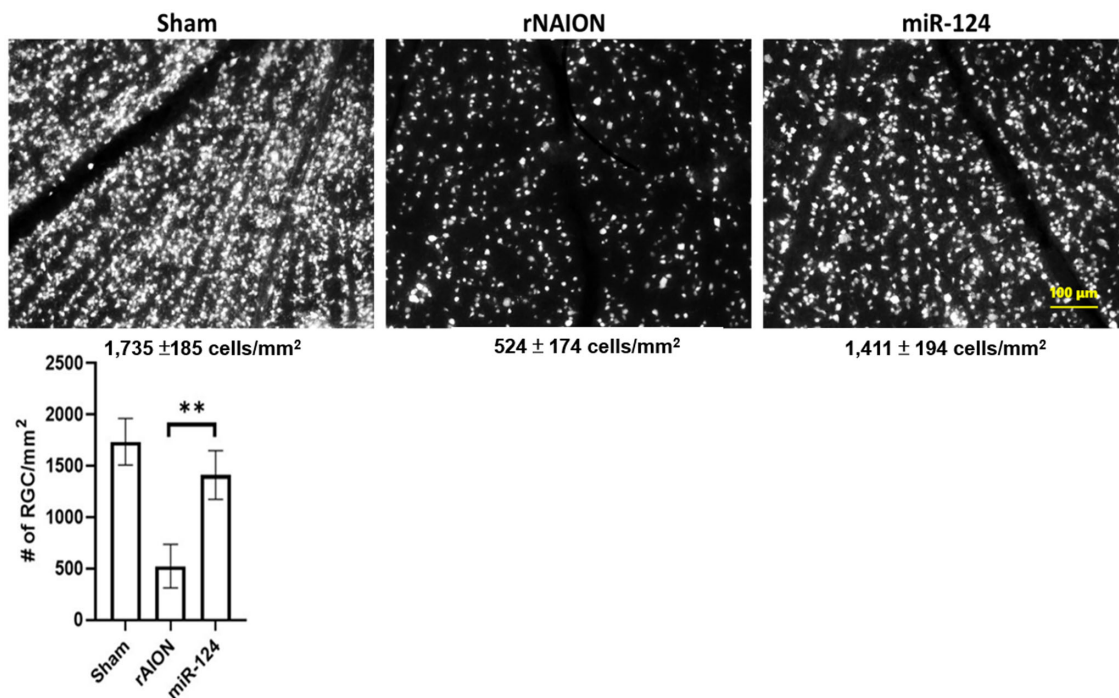


FIGURE 6. RGCs with intact axons were labeled using retrograde fluorescent gold labeling. The density of Fluoro-Gold-labeled RGCs can be used to assess death-free RGCs. The central RGC densities of the sham, rNAION, and miR-124 groups were $1735 \pm 185/\text{mm}^2$, $524 \pm 174/\text{mm}^2$, and $1411 \pm 194/\text{mm}^2$, respectively. Compared with the rNAION group, the miR-124 group had an approximately twofold increase in RGC survival, respectively (** $P < 0.01$, post hoc Dunn's multiple comparison test, $n = 3$ per group).

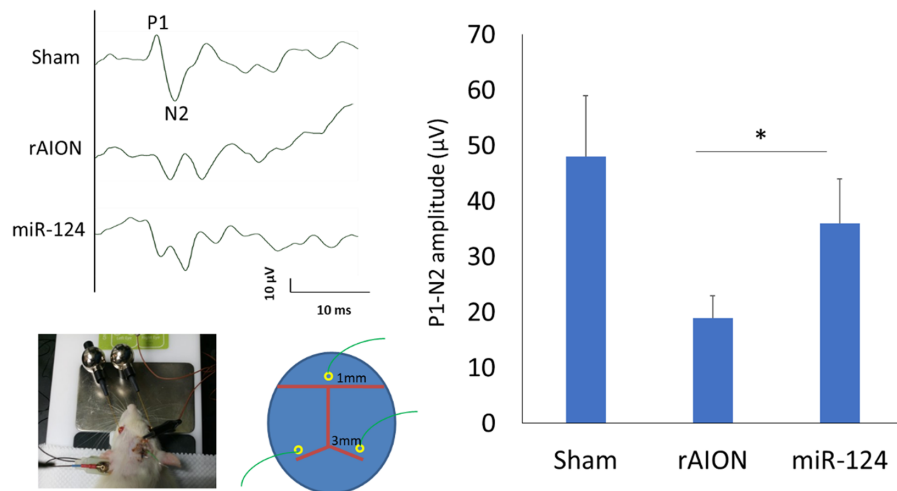


FIGURE 7. A reduction in P1–N2 amplitude indicates that healthy optic nerve axons are stimulated. The mean amplitudes of the P1–N2 waves in the sham, rAION, and miR-124 groups were 48 ± 11 μ V, 19 ± 4 μ V, and 36 ± 8 μ V, respectively. Compared with the rAION group, the amplitudes of the P1–N2 waves were significantly preserved in both the pretreatment and posttreatment groups ($*P < 0.05$, post hoc Dunn's multiple comparison test, $n = 3$ per group).

TABLE 3. RQs Expressed by the Five miRNAs

Relative Quantity (qPCR)	0 h (RQ)	6 h (RQ)	1 d (RQ)	3 d (RQ)	7 d (RQ)
rno-mir-182	6.5058	0.6607	0.0719	2.1172	6.1366
rno-miR-31a-5p	5.5164	0.0604	0.0296	0.0178	7.4236
rno-mir-124-3	7.4355	1.0511	1.7243	2.4023	6.6692
rno-miR-181a-5p	4.0863	0.4905	0.2151	0.1504	3.2532
rno-miR-125a-5p	6.0439	0.1829	0.5589	1.4234	5.2937

3 and recovered on day 7. To verify the miRNA microarray results, we performed RT-qPCR on these five miRNAs (see “RT-qPCR” and Fig. 5) and vision function (see “The Potential Neuroprotective Role of miR-124 in rNAION” and Figs. 6, 7).

RT-qPCR

We selected five miRNA CD63⁺-EVs that were associated with M1 and M2 macrophage modulation for subsequent RT-qPCR analyses. Results were in agreement with the microarray data (Fig. 5). The expression of miR-124-3 was significantly decreased after rNAION induction and returned to the baseline level on day 7. In the microarray assay, there was a dramatic decrease of RQ from 8.30 on day 0 to 1.13 on day 0.25, 1.37 on day 1, and 0.49 on day 3, and it recovered to 5.46 on day 7. It was observed in the transcription fold change to the internal control (GAPDH) of qPCR that RQ decreased from 7.44 (day 0) to 1.05 (day 0.25), 1.72 (day 1), and 2.40 (day 3), and it was also recovered to 6.67 on day 7. The RQs expressed by the other four miRNAs are listed in Table 3. The most dramatic change in miRNA expression from the acute to recovery phase was miR-124, and thus it was selected to test its potential for treating rNAION.

The Potential Neuroprotective Role of miR-124 in rNAION

Rats were randomly assigned to either one of the three groups: sham, rNAION receiving PBS, and rNAION receiving miR-124. Fluoro-Gold-labeled RGC density was assessed in

half of the rats in each group while FVEPs were measured in the other half. The central RGC density in the sham, PBS, and miR-124 groups was $1735 \pm 185/\text{mm}^2$, $524 \pm 174/\text{mm}^2$, and $1411 \pm 194/\text{mm}^2$, respectively (Fig. 6). The density of RGCs in the miRNA-124-treated group still exceeded 80% of that in the sham control group, suggesting the potential neuroprotective effect of miR-124. In contrast, the density of RGCs was reduced to merely 30% in the PBS control group ($P < 0.05$, post hoc Dunn's multiple comparisons test, $n = 3$ in each group). Reduction in the FVEP P1–N2 amplitude indicated a reduced stimulation of healthy optic nerve axons. The mean amplitudes of the P1–N2 wave in the sham, PBS, and miR-124 groups were 48 ± 11 μ V, 19 ± 4 μ V, and 36 ± 8 μ V, respectively (Fig. 7). The amplitudes of the P1–N2 waves were preserved significantly in both the sham and miR-124 treatment groups compared to the control PBS group ($P < 0.05$, post hoc Dunn's multiple comparisons test).

DISCUSSION

In this research, photolabile papers conjugated with CD63 monoclonal antibodies were capable of isolating CD63⁺-EVs from low-volume vitreous humor samples. CD63 is one of the most abundant surface biomarkers localized on extracellular vesicles, particularly exosomes. In the previous research, we were able to extract more than 50% of total miRNAs from CD63⁺-EVs.¹⁷ More important, CD63 is highly expressed within the eye, mainly in the retinal pigment epithelium.¹⁰ It has been found that vitreous humor contains an abundant of EVs, which is reflected by the high concentration of CD63 molecules.^{44,45}

Prior to this study, effective methods to isolate EVs from low-volume samples (<100 μ L), such as embryonic culture medium or ocular fluid, had inconvenient limitations.^{22,46,47} We previously developed a polydimethylsiloxane microfluidic chamber to enrich EVs from conditioned medium and clinical serum samples.¹⁶ However, this device requires a complicated manufacturing process. In this study, the photolabile chips allowed us to successfully profile miRNA expression throughout the recovery period of rNAION. The chromatography paper, composed mainly of cellulose, is a natural three-dimensional microfluidic system that confers more surface for conjugating captured molecules demonstrating a higher efficiency compared to a simple microfluidic channel. It is also low cost, easily stored, ecofriendly, and free from equipment interventions during modifications. A photosensitive linker was used for releasing captured EVs (in Supplementary Table S2). After 30 minutes of the harvesting process, an acceptable amount of CD63⁺-EVs was collected from rNAION samples.

In our previous study, intravitreal injection of G-CSF could significantly inhibit M1-related miRNA signaling in ocular fluids. This process has enhanced the expression of M2-related miRNAs and increased anti-inflammatory proteins, thus promoting optic neuron repair in rNAION.^{2,3,34} The miRNA profiles of the extracted CD63⁺-EVs on day 7 of the natural recovery period were compared with acute-phase samples (days 0.25 to 3). miR-182, miR-31a-5p, miR-124, miR-125a-5p, and miR-181a-5p existence was confirmed using RT-qPCR.

miR-182 is an oxidative stress-related miRNA that directly suppresses TLR4. During the recovery phase, it has the capacity to inactivate NF- κ B and polarize M2 that had been acutely downregulated and then returned to baseline.^{48,49} Inhibition of miR-31a-5p can decrease IL-25 expression to alleviate inflammation. After 7 days of recovery, miR-31a-5p was acutely downregulated.¹¹ Upregulation of miR-125a-5p can diminish M1 polarization and promote IL-4-induced M2 marker expression.⁵⁰ miR-181a-5p overexpression in M1 macrophages may diminish M1 phenotype expression while promoting polarization of the M2 phenotype.⁵¹ miR-124, miR-182, and miR-181a-5p were capable of synchronizing with M2 regulation, resulting in an acute initial downregulation, but slowly proceeded into returning to baseline during the recovery period. During the recovery phase from rNAION, miR-124 showed a significant decrease compared to other miRNAs.

Several circulating and extracellular vesicle-associated miRNAs, including miR-146a, miR-17, miR-125b, and miR-155, have been demonstrated to play a protective role in ischemia-reperfusion injury²⁶ and retinal degeneration.^{10,11} miR-124 is shown to have an increased abundance during anti-inflammation primarily from autocrines such as IL-4 or granulocyte-macrophage colony-stimulating factor in mature M2 macrophages, but not in M0, M1, or M1/M2 macrophages.^{7,26} miR-124 is required for the expression of homeostatic synaptic plasticity, such as alleviating neurodegeneration and preventing cognitive impairment.^{27,28} The downregulation of miR-124 is mainly associated with retinal inflammation and photoreceptor death during retina degeneration, and the upregulation of miR-124 has demonstrated the potential use of miR-124 in humans and rodents.²⁹

The miR-124-3p in EVs is targeted to hippocampal neurons, which reduces neurodegeneration and improves cognition after traumatic brain injury. This identifies miR-124 as a possible treatment that should be explored.²⁷ The

functional study of miR-124 has been confirmed in developing neural differentiation,^{27,29} its role in retinal degeneration has been explored, and the potential use of miR-124 in humans and rodents has been demonstrated. miR-124 mimics can reduce the level of retinal inflammation and photoreceptor cell death, which can greatly contribute to the M2 phenotype of monocytes.⁷ M2 macrophage activation factors may protect optic nerves through miRNAs carried by EVs during the recovery phase.^{2,3,11} Overexpression of miR-124 can reduce the activation of M1 macrophages and promote the M2 regulatory phenotype.²⁶ Inhibition of miR-124 can increase M1 levels, stimulating the body to recycle dead cells and debris, leading to retinal inflammation, photoreceptor death, and retinal degeneration.²⁹

We hypothesize that replenishing miR-124 would reverse the retinal inflammation and protect photoreceptor cells. Synthesized miR-124 molecules were administered intravitreally in rNAION. Results showed miR-124 was capable of protecting visual functions by preventing apoptosis of RGCs. In previous studies, miR-124 sustained homeostatic synaptic plasticity in the neurons and retina. Downregulation of miR-124 caused degeneration in photoreceptor neurons within the inner and outer nuclear layer and the ganglion cell layer.²⁸ During the natural recovery of rNAION, alterations in miR-124 expression were determined from the low-volume vitreous humor of rats using the chip. This was the first in vivo evidence that supported miR-124 as a potential treatment of NAION.

CONCLUSION

NAION can cause permanent visual damage, and there are currently no known effective treatments in the acute phase that can improve outcomes. To study the miRNA profiles during the natural recovery period of rNAION, we developed an efficient and effective photolabile chip technology capable of collecting CD63⁺-EVs from low-volume biosamples (<30 μ L). The chip offers the possibility to clearly extract information from rare biopsy specimens under in vivo conditions and opens up bioinformatic applications. Since miR-124 had the most dramatic change in expression and has been previously described as having anti-inflammatory effects, it was selected as the test drug. rNAION treated with intravitreal injections of miR-124 showed improved RGC survival and visual function, warranting the further exploration of potential neuroprotective effects of miR-124.

Acknowledgments

The authors thank the National Defense Medical Center Instrument Center for technical services.

Supported by grants from Tri-Service General Hospital (TSGH-E-111239) and the Taiwan Ministry of Science and Technology (grant MOST 109-2314-B-007-004).

Disclosure: **Y.-H. Chen**, None; **Y.C. Huang**, None; **C.-H. Chen**, None; **Y.-T. Wen**, None; **R.-K. Tsai**, None; **C. Chen**, None

References

- Bernstein SL, Johnson MA, Miller NR. Nonarteritic anterior ischemic optic neuropathy (NAION) and its experimental models. *Prog Retin Eye Res.* 2011;30(3):167–187.
- Wen YT, Huang TL, Huang SP, et al. Early applications of granulocyte colony-stimulating factor (G-CSF) can stabilize the blood-optic-nerve barrier and ameliorate

- inflammation in a rat model of anterior ischemic optic neuropathy (rAION). *Dis Model Mech*. 2016;9(10):1193–1202.
3. Huang SP, Fang KT, Chang CH, et al. Autocrine protective mechanisms of human granulocyte colony-stimulating factor (G-CSF) on retinal ganglion cells after optic nerve crush. *Exp Eye Res*. 2016;143:132–140.
 4. Lin WN, Kapupara K, Wen YT, et al. *Haematococcus pluvialis*-derived astaxanthin is a potential neuroprotective agent against optic nerve ischemia. *Mar Drugs*. 2020;18(2):85.
 5. Guo Y, Mehrabian Z, Bernstein SL. The rodent model of nonarteritic anterior ischemic optic neuropathy (rNAION). *J Vis Exp*. 2016;(117):54504.
 6. Mehrabian Z, Guo Y, Miller NR, et al. Approaches to potentiated neuroprotective treatment in the rodent model of ischemic optic neuropathy. *Cells*. 2021;10(6):1440.
 7. Veremeyko T, Siddiqui S, Sotnikov I, et al. IL-4/IL-13-dependent and independent expression of miR-124 and its contribution to M2 phenotype of monocytic cells in normal conditions and during allergic inflammation. *PLoS One*. 2013;8(12):e81774.
 8. Théry C, Ostrowski M, Segura E. Membrane vesicles as conveyors of immune responses. *Nat Rev Immunol*. 2009;9(8):581–593.
 9. Théry C, Witwer KW, Aikawa E, et al. Minimal information for studies of extracellular vesicles 2018 (MISEV2018): a position statement of the International Society for Extracellular Vesicles and update of the MISEV2014 guidelines. *J Extracell Vesicles*. 2018;7(1):1535750.
 10. Morris DR, Bounds SE, Liu H, et al. Exosomal miRNA transfer between retinal microglia and RPE. *Int J Mol Sci*. 2020;21(10):3541.
 11. Berber P, Grassmann F, Kiel C, et al. An eye on age-related macular degeneration: the role of microRNAs in disease pathology. *Mol Diagn Ther*. 2017;21(1):31–43.
 12. Liu J, Jiang F, Jiang Y, et al. Roles of exosomes in ocular diseases. *Int J Nanomed*. 2020;15:10519–10538.
 13. Li N, Zhao L, Wei Y, et al. Recent advances of exosomes in immune-mediated eye diseases. *Stem Cell Res Ther*. 2019;10(1):278.
 14. Li DL, Gong YY. A promising strategy for non-arteritic anterior ischemic optic neuropathy: intravitreal mesenchymal stem cell exosome. *Curr Stem Cell Res Ther*. 2021;16(2):109–114.
 15. Rana S, Yue S, Stadel D, et al. Toward tailored exosomes: the exosomal tetraspanin web contributes to target cell selection. *Int J Biochem Cell Biol*. 2012;44(9):1574–1584.
 16. Chen C, Skog J, Hsu CH, et al. Microfluidic isolation and transcriptome analysis of serum microvesicles. *Lab Chip*. 2010;10(4):505–511.
 17. Chen C, Lin BR, Hsu MY, et al. Paper-based devices for isolation and characterization of extracellular vesicles. *J Vis Exp*. 2015;(98):e52722.
 18. Théry C, Amigorena S, Raposo G, et al. Isolation and characterization of exosomes from cell culture supernatants and biological fluids. *Curr Protoc Cell Biol*. 2006;Chapter 3:Unit 3.22.
 19. Chen C, Lin BR, Wang HK, et al. Paper-based immunoaffinity devices for accessible isolation and characterization of extracellular vesicles. *Microfluid Nanofluid*. 2014;16:849–856.
 20. Helwa I, Cai J, Drewry MD, et al. A comparative study of serum exosome isolation using differential ultracentrifugation and three commercial reagents. *PLoS One*. 2017;12(1):e0170628.
 21. Brennan K, Martin K, Fitzgerald SP, et al. A comparison of methods for the isolation and separation of extracellular vesicles from protein and lipid particles in human serum. *Sci Rep*. 2020;10(1):1039.
 22. Lerner N, Avissar S, Beit-Yannai E. Extracellular vesicles mediate signaling between the aqueous humor producing and draining cells in the ocular system. *PLoS One*. 2017;12(2):e0171153.
 23. Wu Y, Li Q, Zhang R, et al. Circulating microRNAs: biomarkers of disease. *Clin Chim Acta*. 2021;516:46–54.
 24. Lerner N, Chen I, Schreiber-Avissar S, et al. Extracellular vesicles mediate anti-oxidative response-in vitro study in the ocular drainage system. *Int J Mol Sci*. 2020;21(17):6105.
 25. Mead B, Tomarev S. Bone marrow-derived mesenchymal stem cells-derived exosomes promote survival of retinal ganglion cells through miRNA-dependent mechanisms. *Stem Cells Transl Med*. 2017;6(4):1273–1285.
 26. Song Y, Li Z, He T, et al. M2 microglia-derived exosomes protect the mouse brain from ischemia-reperfusion injury via exosomal miR-124. *Theranostics*. 2019;9(10):2910–2923.
 27. Ge X, Guo M, Hu T, et al. Increased microglial exosomal miR-124-3p alleviates neurodegeneration and improves cognitive outcome after rmTBI. *Mol Ther*. 2020;28(2):503–522.
 28. Hou Q, Ruan H, Gilbert J, et al. MicroRNA miR124 is required for the expression of homeostatic synaptic plasticity. *Nat Commun*. 2015;6:10045.
 29. Chu-Tan JA, Rutar M, Saxena K, et al. MicroRNA-124 dysregulation is associated with retinal inflammation and photoreceptor death in the degenerating retina. *Invest Ophthalmol Vis Sci*. 2018;59(10):4094–4105.
 30. Mead B, Tomarev S. Extracellular vesicle therapy for retinal diseases. *Prog Retin Eye Res*. 2020;79:100849.
 31. Lu L, McCurdy S, Huang S, et al. Time series miRNA-mRNA integrated analysis reveals critical miRNAs and targets in macrophage polarization. *Sci Rep*. 2016;6:37446.
 32. Huang TL, Huang SP, Chang CH, et al. Factors influencing the retrograde labeling of retinal ganglion cells with fluorogold in an animal optic nerve crush model. *Ophthalmic Res*. 2014;51(4):173–178.
 33. Huang TL, Huang SP, Chang CH, et al. Protective effects of systemic treatment with methylprednisolone in a rodent model of non-arteritic anterior ischemic optic neuropathy (rAION). *Exp Eye Res*. 2015;131:69–76.
 34. Huang TL, Wen YT, Chang CH, et al. Early methylprednisolone treatment can stabilize the blood-optic nerve barrier in a rat model of anterior ischemic optic neuropathy (rAION). *Invest Ophthalmol Vis Sci*. 2017;58(3):1628–1636.
 35. Pahattuge TN, Jackson JM, Digamber R, et al. Visible photorelease of liquid biopsy markers following microfluidic affinity-enrichment. *Chem Commun (Camb)*. 2020;56(29):4098–4101.
 36. Shin DS, Seo JH, Sutcliffe JL, et al. Photolabile micropatterned surfaces for cell capture and release. *Chem Commun (Camb)*. 2011;47(43):11942–11944.
 37. LeValley PJ, Neelarapu R, Sutherland BP, et al. Photolabile linkers: exploiting labile bond chemistry to control mode and rate of hydrogel degradation and protein release. *J Am Chem Soc*. 2020;142(10):4671–4679.
 38. Sewer A, Gubian S, Kogel U, et al. Assessment of a novel multi-array normalization method based on spike-in control probes suitable for microRNA datasets with global decreases in expression. *BMC Res Notes*. 2014;7:302.
 39. Kim A, Saikia P, Nagy LE. miRNAs involved in M1/M2 hyperpolarization are clustered and coordinately expressed in alcoholic hepatitis. *Front Immunol*. 2019;10:1295.
 40. Essandoh K, Li Y, Huo J, et al. MiRNA-mediated macrophage polarization and its potential role in the regulation of inflammatory response. *Shock*. 2016;46(2):122–131.
 41. Chang CH, Huang TL, Huang SP, et al. Neuroprotective effects of recombinant human granulocyte colony-

- stimulating factor (G-CSF) in a rat model of anterior ischemic optic neuropathy (rAION). *Exp Eye Res.* 2014;118:109–116.
42. Shapouri-Moghaddam A, Mohammadian S, Vazini H, et al. Macrophage plasticity, polarization, and function in health and disease. *J Cell Physiol.* 2018;233(9):6425–6440.
 43. Taj SH, Kho W, Riou A, et al. MiRNA-124 induces neuroprotection and functional improvement after focal cerebral ischemia. *Biomaterials.* 2016;91:151–165.
 44. Kang M, Ryu J, Lee D, et al. Correlations between transmembrane 4 L6 family member 5 (TM4SF5), CD151, and CD63 in liver fibrotic phenotypes and hepatic migration and invasive capacities. *PLoS One.* 2014;9(7):e102817.
 45. Dismuke WM, Challa P, Navarro I, et al. Human aqueous humor exosomes. *Exp Eye Res.* 2015;132:73–77.
 46. Mead B, Tomarev S. Retinal ganglion cell neuroprotection by growth factors and exosomes: lessons from mesenchymal stem cells. *Neural Regen Res.* 2018;13(2):228–229.
 47. Rudraprasad D, Rawat A, Joseph J. Exosomes, extracellular vesicles and the eye. *Exp Eye Res.* 2022;214:108892.
 48. Wang Y, Zhao X, Wu X, et al. MicroRNA-182 mediates Sirt1-induced diabetic corneal nerve regeneration. *Diabetes.* 2016;65(7):2020–2031.
 49. Muraleedharan CK, McClellan SA, Ekanayaka SA, et al. The miR-183/96/182 cluster regulates macrophage functions in response to *Pseudomonas aeruginosa*. *J Innate Immun.* 2019;11(4):347–358.
 50. Banerjee S, Cui H, Xie N, et al. MiR-125a-5p regulates differential activation of macrophages and inflammation. *J Biol Chem.* 2013;288(49):35428–35436.
 51. Bi J, Zeng X, Zhao L, et al. MiR-181a induces macrophage polarized to M2 phenotype and promotes M2 macrophage-mediated tumor cell metastasis by targeting KLF6 and C/EBP α . *Mol Ther Nucleic Acids.* 2016;5(9):e368.